Dislocation array elements for the analysis of crack and yielded zone growth

N. J. MILLS

Department of Physical Metallurgy, University of Birmingham, Birmingham, UK

Stress fields were found for boundary elements that consist of linear arrays of disloca-tions, or arrays of dislocations that simulate a crack tip. A number of two-dimensional elastic boundary value problems were solved using these elements. Crack growth paths were predicted for pairs of interacting cracks and the energetics of multiple crack growth away from a free surface was analysed. In certain simple elastic—plastic problems, where the general shape of the plastic zone is known, the plastic zone size was predicted.

1. Introduction

Several simple crack problems have been solved analytically using continuous distributions of edge dislocations as a way of modelling the stress conditions at the crack surfaces [1, 2]. However, many crack problems of interest are geometrically more complex than this and hence cannot easily be solved analytically; for example, the crack may be curved, there may be several interacting or branched cracks, and the specimen boundaries may not lie at infinity. To deal with such problems numerical methods of solution using boundary elements have been developed.

Crouch [3] and Markinowski [4] have devel-oped constant displacement elements based on a finite number of edge dislocations around the boundary of the body, see Fig. 1a. Such simple elements produce an acceptable model but there are several disquieting factors that limit its appli-cability. Firstly, it will be shown later that the tensile stress normal to the element, when averaged over the element length, has an infinite value; hence, evaluating the stress at the mid-point of the segment [3] may lead to significant errors. Secondly, the stress field close to the ends of the elements will be inaccurate, though that present at a distance from the elements will be acceptable by St Venant's principle. The stress field near the end of a crack needs to be evaluated if crack growth directions are to be predicted, so for this purpose crack tip elements are almost essential.

The stress field of an edge dislocation and a point force in a plane are similar in many ways [5, 6] so that boundary elements using a single point force on each element [7], are similar in capabilities to constant displacement elements. Isida [8] has described briefly the use of a linear array of pairs of point forces. It should be noted that he has changed the intervals for evaluating the stress boundary conditions from the natural ones of each element because the number of unknown element parameters must equal the number of boundary stress conditions.
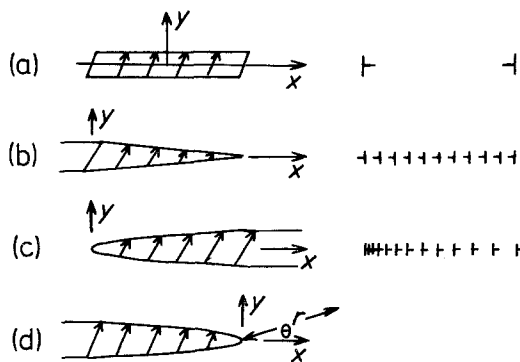

Figure 1 Boundary elements used: (a) constant displace-ment discontinuity between $(-a, 0)$ and $(a, 0)$. (b) to (d) halves of the linear and crack-tip elements, having (b) a linear and (c and d) a parabolic variation in the displacement discontinuity. The sketches on the right indicate the equivalent edge dislocation, each of which has a complex Burger's vector.
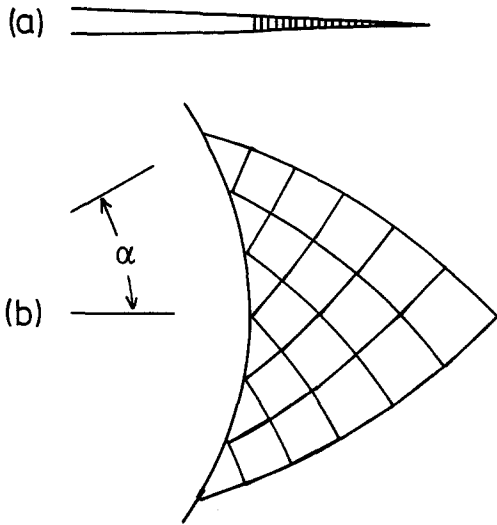
Figure 2 (a) A line yielded zone at a crack tip. (b) A slip line field yielded zone at a circular notch of maximum extent α.

In dealing with crack problems, the two main linear elastic fracture mechanics parameters are the so-called strain energy release rate, G, (strictly it is a potential energy release rate) and the stress intensity factor, K. In strictly elastic problems, G can be evaluated from a boundary integral of the potential energy changes when the crack grows. If there is a plastic zone in the material that does not surround the crack tip, then the potential energy release rate from the elastic region may not be meaningful in fracture mechanics terms, so then it may be necessary to estimate K directly from the crack shape near the crack tip, since the potential energy calculation for the whole boundary may become doubtful. Hence, a crack tip displacement element has been introduced (Fig. 1c). Alternatively, if the yielded zone encompasses the crack or notch tip there will be further difficulties in evaluating suitable fracture mechanics parameters (Fig. 2). In this case it is often necessary to examine the particular materials being tested to see what kind of plasticity occurs: for example, the line-yielded zone shown in Fig. 2a is a good model of craze yielding at a crack tip in certain polymers, and the more complex zone shown in Fig. 2b, based on a slip line field analysis, has sometimes been observed [9].

2. Theory
2.1. Elements used and their stress fields
The complex variable stress functions, introduced by Muskhelishvili [10], are used, in which the combinations Θ and Φ of the stress components σ_{xx}, σ_{yy} and σ_{xy} in the xy-plane, and the displacements components U_x and U_y are calculated from the two analytic functions $\phi(Z)$ and $\psi(Z)$ (where $z = x + iy$) using the expressions

$$\Theta \equiv \tfrac{1}{2}(\sigma_{xx} + \sigma_{yy}) = 2\,\mathrm{Re}\,\phi'(Z); \quad (1)$$

$$\Phi \equiv \tfrac{1}{2}(\sigma_{yy} - \sigma_{xx} + 2i\sigma_{xy})$$
$$= \bar{Z}\phi''(Z) + \psi'(Z); \quad (2)$$

$$2G(U_x + iU_y) = \kappa\phi(Z) - Z\overline{\phi'(Z)} - \overline{\psi(Z)}, \quad (3)$$

where the elastic constants are G, the shear modulus and κ, which is equal to $(3-4\nu)$, where ν is Poisson's ratio (for plane strain deformation) and the primes denote differentiation with respect to Z, and the bars indicate complex conjugates.

2.1.1. The constant displacement element
The stress function for this element is first found for the simple case where the displacement discontinuity of magnitude $b_x + ib_y$ occurs along the x-axis from $-a$ to $+a$ (Fig. 1a). The element can be decomposed into two generalized edge dislocations. The stress functions for such a dislocation, with a displacement discontinuity of $b_x + ib_y$ running from a to $-\infty$ along the x-axis are [11]:

$$\phi_0(Z) = \gamma \ln(Z - a) \quad (4)$$

$$\psi_0(Z) = \bar{\gamma} \ln(Z - a) - \frac{\gamma a}{Z - a}, \quad (5)$$

where $\gamma = G(b_x + ib_y)/4i\pi(1 - \nu)$. The element can thus be made up of a "dislocation" of magnitude γ ending at a, and a "dislocation" of magnitude $-\gamma$ ending at $-a$. When the appropriate stress functions are added, and substituted into Equations 1 and 2 the resulting stress field can be evaluated from

$$\Theta = 2\,\mathrm{Re}\left[\gamma\left(\frac{1}{Z - a} - \frac{1}{Z + a}\right)\right]; \quad (6)$$

and

$$\Phi = \bar{\gamma}\left(\frac{1}{Z - a} - \frac{1}{Z + a}\right)$$
$$- \gamma\left(\frac{\bar{Z} - a}{(Z - a)^2} - \frac{\bar{Z} + a}{(Z + a)^2}\right). \quad (7)$$

Note that, in a Mohr circle diagram for stress components, the real function, Θ, represents the position of the centre of the circle along the tensile stress axis and the complex function, Φ, represents the vector from the centre of the Mohr
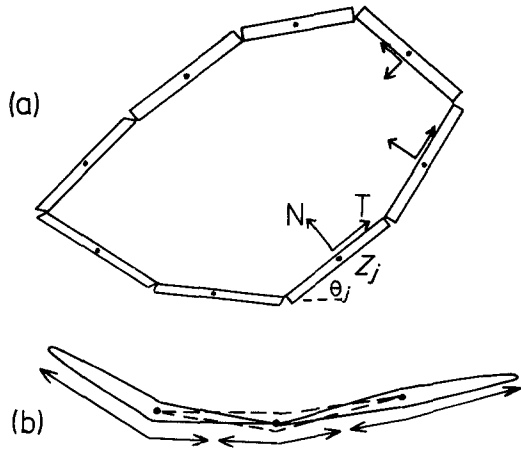
Figure 3 (a) The boundary of a body represented by straight segments, using constant displacement elements. (b) A crack represented by 2 crack-tip elements and a linear element (the double headed arrows indicate the limits of integration for averaging the boundary stresses).

circle to the point $(\sigma_{yy}, \sigma_{xy})$ on the circle. Hence, a rotation of co-ordinate axes by the angle θ leaves Θ unchanged, whereas the vector representing Φ is rotated by an angle 2θ.

If the constant displacement element is moved to a general position in the Z-plane with its centre at Z_j and its orientation specified by the complex number $T_j = e^{i\theta_j}$ (Fig. 3a), then the simplest way to evaluate the stress components at a point Z is to use the co-ordinate transformation, W, where

$$W = (Z - Z_j)/T_j, \qquad (8)$$

so that the element is at the centre of the W plane. Equations 6 and 7 can then be used to evaluate Θ_W and Φ_W if the symbol Z is replaced by the symbol W throughout. Finally the stress components must be restored to the Z-axes using

$$\Theta_Z = \Theta_W \qquad (9)$$

and

$$\Phi_Z = \Phi_W/T_j^2. \qquad (10)$$

Note that, if γ is defined, before the co-ordinate transformation from the Z to the W axes, as C or $-iC$, where C is the real constant $G/4\pi(1 - \nu)$, and if its value is used unaltered in evaluating Θ_W and Φ_W, then it represents a unit normal or unit tangential displacement discontinuity in the W axes of the element.

One problem with the constant element can be seen by evaluating the stress component normal to it, along the x-axis. Since

$$\sigma_{yy} = \Theta + \text{Re } \Phi \qquad (11)$$

when $Z = x$, from Equations 6 and 7,

$$\sigma_{yy} = \frac{4ab_y C}{x^2 - a^2}. \qquad (12)$$

There is a singularity in σ_{yy} at $x = \pm a$. The value at the centre of the element $\sigma_{yy}(x = 0) = -4b_y C/a$ can be used for evaluating stress boundary conditions, however, the average value of σ_{yy} over the length of the element $a > x > -a$ is infinite.

2.1.2. The linear element

The linear element (see Fig. 1b) can again be made out of generalized edge dislocations. If the displacement discontinuity at the origin is $b_x + ib_y$, and this tapers linearly to zero at $x = a$, then Equations 4 and 5 can be multiplied by the density function $\rho(x)$, where

$$\rho(x) = 1/a \qquad \text{for } a > x > 0$$

$$= 0 \qquad \text{for } x < 0 \text{ or } x > a, \qquad (13)$$

and integrated over the limits $\infty > x > -\infty$ to give

$$\phi(Z) = \frac{1}{a} \int_0^a \gamma \ln (Z - x) \, dx$$

$$= \gamma \ln (Z - a) - \frac{\gamma Z}{a} \ln \left(\frac{Z - a}{Z}\right) - \gamma. \qquad (14)$$

If a similar process is carried out for $\psi(Z)$, and then Equations 1 and 2 are applied, the resulting stress field is given by

$$\Theta = \text{Re} \left[-\frac{2\gamma}{a} \ln \left(\frac{Z - a}{Z}\right)\right]; \qquad (15)$$

$$\Phi = \frac{(\gamma - \bar{\gamma})}{a} \ln \left(\frac{Z - a}{Z}\right) + \frac{\gamma(Z - \bar{Z})}{Z(Z - a)}. \qquad (16)$$

Note that the linear displacement discontinuity in Fig. 1b has not been terminated by adding a dislocation of magnitude $-(b_x + ib_y)$ at the origin, and therefore it extends to $-\infty$ along the x-axis. This dislocation must be added if the displacement field of the element is to be evaluated, but if only the stress field is evaluated it may be ignored. This is because the complete element consists of two adjoining linear wedges (Fig. 3b) and the stress fields of the edge dislocations where the wedges join cancel out.

For a single linear wedge along the x-axis, the stress components normal to its length, $\sigma_N (= \sigma_{yy})$, and tangential to its length, $\sigma_T (= \sigma_{xy})$, can be evaluated as, respectively,
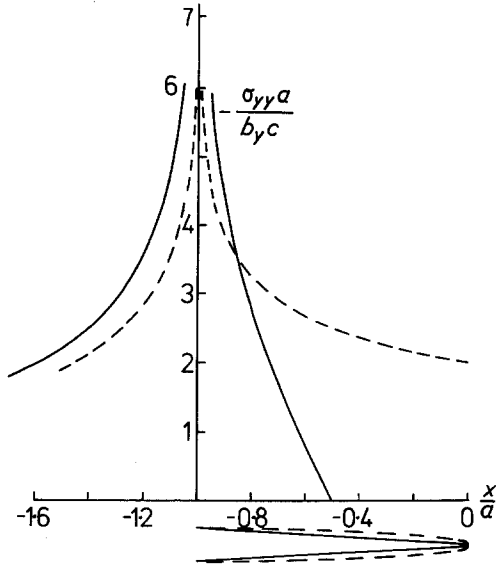
Figure 4 — $\sigma_{yy}a/b_yC$ plotted against x/a. The solid line shows the variation in compressive stress normal to a half linear element such as that shown in Fig. 1b and the dashed line shows the variation in compressive stress normal to a half crack-tip element such as that shown in Fig. 1d.

$$\sigma_{yy} = -\frac{2b_yc}{a} \ln \left(\frac{a-x}{x} \right) \qquad (17)$$

and

$$\sigma_{xy} = -\frac{2b_xc}{a} \ln \left(\frac{a-x}{x} \right). \qquad (18)$$

The variation of stress normal to the length is shown in Fig. 4. The average normal stress is evaluated to find the influence coefficients of the elements. For example,

$$\bar{\sigma}_{yy} \left(\frac{a}{2} > x > 0 \right) = \frac{2}{a} \int_0^{a/2} \sigma_{yy}(x) \, dx$$

$$= -\frac{4b_yC}{a} \ln 2 \qquad (19)$$

and

$$\bar{\sigma}_{yy} \left(0 > x > -\frac{a}{2} \right) = -\frac{2b_yC}{a} \ln (27/4). \quad (20)$$

Note that the average value of σ_{yy} in the interval $a > x > 0$ is zero; so that if the boundary intervals for integration are chosen to coincide with the boundary segments, the self influence coefficients are zero. Later, this will be shown to lead, in some circumstances, to oscillatory solutions.

2.1.3. The crack tip element

Fig. 1c shows the crack tip element, which has its tip at the origin, and for which the displacement discontinuity builds up to $b_x + ib_y$ at $x = a$.

Providing that only the stress field is required, it can be made up from the "dislocations" of Equations 4 and 5 using a dislocation density, $\rho(x)$, such that

$$\rho(x) = -\frac{1}{2\sqrt{ax}} \qquad \text{for } a > x > 0$$

$$= 0 \qquad \text{for } x > a \text{ or } x < 0, \quad (21)$$

to give the required parabolic crack-tip profile. Combining Equations 4 and 5 and 21 gives the stress function

$$\phi'(Z) = \int_0^a \rho(x)\dot{\phi}_0'(Z) \, dx$$

$$= -\frac{\gamma}{2} \int_0^a \frac{1}{(aZ)^{1/2}} \frac{dx}{(Z-x)}$$

$$= -\frac{\gamma}{2(aZ)^{1/2}} \log \left(\frac{(Z)^{1/2} + (a)^{1/2}}{(Z)^{1/2} - (a)^{1/2}} \right). \qquad (22)$$

Therefore,

$$\Theta = \text{Re} \left[-\frac{\gamma}{(aZ)^{1/2}} \log \left(\frac{(Z)^{1/2} + (a)^{1/2}}{(Z)^{1/2} - (a)^{1/2}} \right) \right]. \qquad (23)$$

Similarly,

$$\Phi = \frac{(\gamma + \gamma\bar{Z}/Z - 2\bar{\gamma})}{4(aZ)^{1/2}} \log \left(\frac{(Z)^{1/2} + (a)^{1/2}}{(Z)^{1/2} - (a)^{1/2}} \right)$$

$$+ \frac{\gamma}{2} \left(1 - \frac{\bar{Z}}{Z} \right) \frac{1}{(a-Z)} \qquad (24)$$

For a crack-tip element running from $-a$ to 0, Fig. 1d, Equations 23 and 24 can still be used since

$$\Theta_{\text{left}}(a, \gamma, Z) = \Theta_{\text{right}}(a, \gamma, -Z) \qquad (25)$$

and

$$\Phi_{\text{left}}(a, \gamma, Z) = \Phi_{\text{right}}(a, \gamma, -Z), \qquad (26)$$

where "left" and "right" refer to Fig. 1c and d, respectively.

From Equations 23 and 24, the tensile stress normal to the crack-tip element can be evaluated as

$$\sigma_{yy} \Big|_{y=0} = -\frac{b_yC}{a(\nu)^{1/2}} \log \left| \frac{(\nu)^{1/2} + 1}{(\nu)^{1/2} - 1} \right|, \quad (27)$$

when $Z = \nu a$ and $0 < \nu < 1$. Fig. 4 shows how this normal stress varies along the length of the element. As the crack tip is approached the stress σ_{yy} tends asymptotically to the value $-2b_yC/a$.

2.1.4. Infinite array of constant displacement elements in a semi-infinite sheet

These elements will be used to model infinite arrays of edge cracks (or crazes) that are all normal
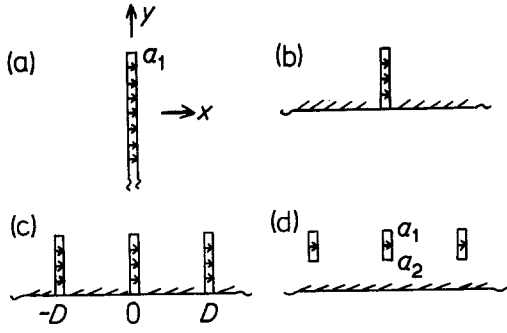
Figure 5 Elements for modelling an infinite array of edge cracks. (a) A single edge dislocation. (b) An edge dislocation with an image dislocation and shear stresses on $y = 0$, i.e., an edge dislocation in a half plane. (c) The edge dislocation in a half plane (as in b) is repeated at intervals of D to give an infinite array of dislocations. (d) A further array added to that of (c) to complete the elements.

to the free surface of a semi-infinite sheet. Fig. 5 shows the process of building up the stress functions of the elements. Because of the mirror plane normal to the free surface the displacement discontinuity has a single component b_x normal to its length. In Fig. 5a there is a single edge dislocation of "Burger's vector" b_x situated at $(0, a)$, and the stress functions for this are

$$\phi_a(Z) = ib_xC \ln\left[-i(Z - ia)\right] \quad (28)$$

and

$$\psi_a(Z) = ib_xC \ln\left[-i(Z - ia)\right] - \frac{ab_xC}{Z - ia}, \quad (29)$$

where $C = G/4\pi(1 - \nu)$, as before.

Fig. 5b shows the same edge dislocation in the half-plane $y > 0$. Using the method of analytic continuation across the y-axis [12], the stress functions in the half-plane that will give $\sigma_{yy} = \sigma_{xy} = 0$ on the y-axis are

$$\phi_b(Z) = \phi_a(Z) - Z\overline{\phi_a'(\overline{Z})} - \overline{\psi_a(\overline{Z})} \quad (30)$$

and

$$\psi_b(Z) = \psi_a(Z) + Z\overline{\psi_a'(\overline{Z})} - \overline{\phi_a(\overline{Z})}$$
$$+ Z\overline{\phi_a'(\overline{Z})} + Z^2\overline{\phi_a''(\overline{Z})} \quad (31)$$

When Equations 28 and 29 are substituted in Equations 30 and 31, respectively, and the stress components evaluated using Equations 1 and 2, the results are

$$\Theta_b(Z) = -2b_xC\left[\text{Im}\left(\frac{1}{Z_1} - \frac{1}{Z_2}\right) + 2a\,\text{Re}\left(\frac{1}{Z_2^2}\right)\right] \quad (32)$$
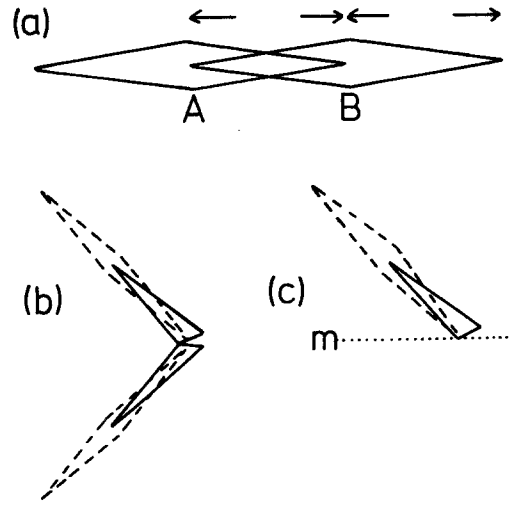

Figure 6 Details of linear boundary element modelling. (a) Two elements, and the integration intervals for stresses (double head arrows) that lead to oscillatory solutions. (b) Special elements, consisting of a single array to dislocations, at sharp corners of the boundary. (c) Sharp corners produced by planes of symmetry.

and

$$\Phi_b(Z) = -2ib_xC\left[\frac{1}{Z_1} - \frac{iy_2}{Z_1^2} - \frac{1}{Z_2} + \frac{iy_2}{Z_2^2} + \frac{4ay}{Z_2^3}\right], \quad (33)$$

where $Z_1 = Z - ia$ and $Z_2 = Z + ia$ and $y_1 = y - a$ and $y_2 = y + a$. In both Equations 32 and 33 the first term is the contribution of a dislocation at $(0, a)$ in an infinite plate, the second term is the "image" dislocation at $(0, -a)$ in an infinite plate and the final term is the correction term to make the x-axis free of stress components σ_{yy} or σ_{xy}. σ_{yy} or σ_{xy}.

In Fig. 5c the dislocations in Fig. 6b have been reproduced at intervals D along the x-axis. Now,

$$\phi_b'(Z) = ib_xC\left(\frac{1}{Z_1} - \frac{1}{Z_2}\right) - \frac{2ab_xC}{Z_2^2} \quad (34)$$

and so

$$\phi_c'(Z) = ib_xC\left(\sum_{n=-\infty}^{\infty}\frac{1}{Z_1 - nD} - \sum_{n=-\infty}^{\infty}\frac{1}{Z_2 - nD}\right)$$
$$- 2ab_xC\sum_{n=-\infty}^{\infty}\frac{1}{(Z_2 - nD)^2}. \quad (35)$$

The sum of the series are given by [13]

$$\sum_{n=-\infty}^{\infty}\frac{1}{Z - nD} = \frac{\pi}{D}\cot\left(\frac{\pi Z}{D}\right). \quad (36)$$

1321

So, differentiating both sides of Equation 36, gives

$$\sum_{n=-\infty}^{\infty} \frac{1}{(Z-nD)^2} = \frac{\pi^2}{D^2} \csc^2\left(\frac{\pi Z}{D}\right). \quad (37)$$

$$\phi_C'(Z) = \frac{ib_x C\pi}{D}\left[\cot\left(\frac{\pi Z_1}{D}\right) - \cot\left(\frac{\pi Z_2}{D}\right)\right]$$
$$- 2ab_x C\frac{\pi^2}{D^2}\csc^2\left(\frac{\pi Z_2}{D}\right) \quad (38)$$

and

$$\Theta_C = -2b_x C\frac{\pi}{D}\left\{\text{Im}\left[\cot\left(\frac{\pi Z_1}{D}\right) - \cot\left(\frac{\pi Z_2}{D}\right)\right]\right.$$
$$\left. - 2\frac{a\pi}{D}\text{Re}\left[\csc^2\left(\frac{\pi Z_2}{D}\right)\right]\right\}. \quad (39)$$

Similarly, the second combination of stress components can be evalulated as

$$\Phi_C(Z) = -\frac{2ib_x C\pi}{D}\left[\cot\left(\frac{\pi Z_1}{D}\right) - iy_1\csc^2\left(\frac{\pi Z_1}{D}\right)\right.$$
$$- \cot\left(\frac{\pi Z_2}{D}\right) + iy_2\csc^2\left(\frac{\pi Z_2}{D}\right)$$
$$\left. + \frac{4ay\pi}{D}\cot\left(\frac{\pi Z_2}{D}\right)\csc^2\left(\frac{\pi Z_2}{D}\right)\right]. \quad (40)$$

Note the close similarity in form of Equations 39 and 40 and Equations 32 and 33.

Finally, Fig. 5d shows the complete constant element inside the repeating strip $\pi/2 > \text{Re } W > -\pi/2$. Equations 39 and 40 can be used twice, for a dislocation of Burgers vector b_x at $(0, a_1)$ and a dislocation $-b_x$ at $(0, a_2)$, in order to build up the element. Transformation to the reduced variable $W = \pi Z/D$ simplifies Equations 39 and 40.

2.2. Influence coefficients and the solution of the boundary value problem
2.2.1. Influence coefficients for constant elements
When constant elements are used, the boundary stresses are usually only evaluated at the midpoint of each element, as in [3]. Fig. 3a shows that there is a one-to-one correspondence between the number of elements and the number of boundary conditions, whether the boundary is open (for cracks etc.) or closed. There are two unknowns for each element (the normal and tangential component of the displacement discontinuity) and there are two boundary conditions at each mid-point (the shear stress and the tensile stress

normal to the boundary). If there are n boundary elements then there are $2n$ unknown displacement components x_j and $2n$ known boundary stress components B_i. These are related by influence coefficients F_{ij} such that

$$F_{ij}x_j = B_i, \quad (41)$$

where the Einstein repeated suffix convention implies the summation for $j = 1 \ldots 2n$. The influence coefficient, F_{ij}, is the stress component at the centre of the ith element due to a unit displacement component at the jth element. From Equation 12 the self influence coefficients F_{ii} are equal to $-4C/a$ when both the stress and the displacement are shear or normal to the element, and are otherwise equal to zero. Note that it would be impossible to use the average stress component along each boundary element in the calculation, because the self-influence coefficients would be infinite.

Equation 41 is solved by Gaussian elimination, the number n usually being restricted to less than 50 by considerations of available computer time.

2.2.2. Influence coefficients for linear or crack-tip elements
When crack-tip or linear elements are used, the first problem that arises when the boundary is open is that the number of elements is one less than the number of straight-line segments into which the boundary is divided (Fig. 3b). This problem has been overcome by evaluating the average boundary stress components over intervals that stretch from adjacent segment mid-points (as in [8]). Another reason for adopting this method is shown in Fig. 6a, where just two collinear elements are shown. On the central boundary AB (in Fig. 6a) the average stress component due to the right-hand wedge of Element 1, or the left-hand wedge of Element 2, is zero. If the segments are of equal length, the influence coefficient for Element 1 is that of its left-hand wedge, and this is equal and opposite to the influence coefficient of Element 2. Hence, if the displacements at the centres of Elements 1 and 2 are equal and opposite there would be a zero average stress component on AB. It was found that when boundary intervals such as AB were used with a larger number of elements, oscillatory solutions often occurred, with the displacement being alternatively large and positive and then large and negative at neighbouring elements.

If the boundary contains right-angled corners, as is common with closed boundary problems, it was found necessary to allow separate unknown displacements on either side of the corner, as in Fig. 6b, with the appropriate stress integration intervals. Similarly, if symmetry operators are used to reduce the length of the boundary being considered, it may be necessary to use a half-element at the end of the boundary (Fig. 6c). Reflection in the x- and y-axes can then be used to build up the total boundary.

The average stress components on each boundary segment were found by evaluating the stress component at four points on each boundary, using positions and weighing factors from the Gaussian numerical integration method, as in [7]. This would give an exact answer if the stress component was a polynomial function, of degree $\leqslant 7$, of position. However, either along or near a boundary element the stresses vary more rapidly than can be accurately represented by a 7th order polynomial, see Fig. 4. Hence, it is necessary to calculate the influence coefficients analytically for both self-influence coefficients and for the influence of an element on its nearest neighbour, if small errors are not to be introduced into the solution. Equations 19 and 20 have already given some of the self-influence coefficients for linear elements, and further of these coefficients are listed in Table I. In the evaluation of influence coefficients, each straight boundary segment is examined in turn so the two halves of each element will be considered separately. If neighbouring segments are not collinear, or not equal in length, then the asterisked values in Table I do not apply;

instead a correction factor is used to bring the Gaussian integration calculation up to the analytic integration value for the case of collinear equal-length segments and then this correction-factor is used subsequently for other cases.

2.3. Removing any stress at infinity

For cracked infinite or semi-infinite bodies it is difficult to arrange for boundary elements to apply the stresses at infinity. Consequently such problems are decomposed into two parts:

(a) an infinite sheet having uniform stresses of σ_{yy}^{∞} σ_{xx}^{∞} σ_{xy}^{∞} everywhere;
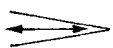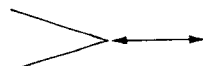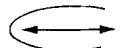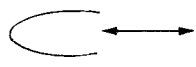
(b) a cracked infinite sheet which is stress-free at infinity; on the crack surfaces additional stress components σ_{N} and σ_{T} have been added.

When Parts a and b are superimposed, the sum of the normal and tangential stress components at the crack surfaces adds up to zero.

When the crack growth is being modelled under constant applied stress conditions, then there are no energy changes in sub-problem a, hence the energy changes in sub-problem b can be used to calculate fracture mechanics parameters.

The situation when dealing with craze growth problems (a craze is a crack-shaped yielded zone which transmits a tensile stress normal to its surface, typically found in glassy plastics) is more complex. If it is assumed that the only plastic deformation occurs inside the craze, then stored elastic energy calculations from sub-problem b still give the change of potential energy in the elastic region. However the plastic energy dissipation in the craze must be calculated using the original tensile stresses across the craze.

TABLE I Self-influence coefficients

Type of half-element	Boundary length	Shape of element	$\dfrac{\overline{\sigma_{yy}}}{b_y}$ or $\dfrac{\overline{\sigma_{xy}}}{b_x}$
Linear	Half of same segment		$\pm\,4C\ln 2/a$
Linear	Adjoining half of * next segment		$\pm\,2C\ln(6.75)/a$
Linear	Whole of next segment * (which is a crack tip)		$\pm\,4C\ln 2/a$
Crack tip	Whole of next segment		$-\,4C\ln 2/a$
Crack tip	Adjoining half of * next segment		$-\,2.9128\,C/a$

*These values apply only if the adjoining segments are collinear and both of length a.

2.4. Prediction of crack growth direction

There are two main criteria that can be used to predict the direction of crack growth [14]. One postulates that the crack will grow in the direction in which the stress component $\sigma_{\theta\theta}$ (in polar coordinates based on the crack tip) has the maximum tensile value. The other postulates that the crack grows along the radial direction in which the strain energy density is a minimum. Sih [14] compared predictions based on these two criteria with experimental results on the growth direction from angled cracks in glassy polymethyl methacrylate (PMMA) and showed that, although both gave reasonable results, the strain energy criterion gave a slightly better prediction. There are a number of points that should be made clear before rejecting the maximum stress criterion, however; in real materials, like PMMA, yielding (in this case craze growth) preceeds crack growth, and if the growing crack follows the craze then perhaps the experiment tests the growth direction predictions for craze growth [15]. Also the direction of the maximum $\sigma_{\theta\theta}$ value varies strongly with radial distance from the crack tip in the elastic stress field; in the experiment the crack growth direction changes rapidly in the initial stages of growth. Hence, the errors in measuring the growth direction after a very small growth increment of, for example, 0.1 mm are large.

The maximum stress crack growth direction criterion has been used in this work because it is easier to put it into effect in the computer programme. If a crack tip element is used, of length a, the boundary element solution gives the values of the displacement components b_N and b_T normal and tangential to its length at the open end of the element. From these the stress intensity factors K_I for crack opening and K_{II} for crack-in-plane sliding can be calculated using

$$K_I + iK_{II} = C\sqrt{2\pi/a}\,(b_N + ib_T). \qquad (42)$$

For mixed-mode loading the stress field adjacent to the crack tip is dominated by the K_I and K_{II} terms and the maximum $\sigma_{\theta\theta}$ value occurs when $\sigma_{r\theta} = 0$ or when

$$K_I \sin\theta + K_2(3\cos\theta - 1) = 0, \qquad (43)$$

where θ is defined in Fig. 1d. In the computer program, once the ratio K_I/K_{II} is calculated, Equation 43 is solved numerically by the Newton–Raphson method (this seems to be the most reliable way of getting to the maximum tensile stress position by the quickest route).

When only linear elements, or constant elements are used around the crack boundary (as when craze growth in polymers is being modelled), the stress component $\sigma_{\theta\theta}$ has to be evaluated at a given radial distance from the final element end, and the maximum position found by a binary search method.

2.5. Energy changes as a consequence of crack or yielded zone growth

2.5.1. Calculation of potential energy changes

The potential energy per unit thickness of a planar body, V, is defined, in the absence of body forces, by

$$V = \int_\tau U \, dA - \int_\Sigma \mathbf{T}.\mathbf{U} \, ds, \qquad (44)$$

where the strain energy density, U, is integrated over all the elements of area dA in the body, τ, and the product of surface traction $\mathbf{T}$ and the surface displacement vector $\mathbf{U}$ is integrated over the elements ds of the perimeter Σ. If only tractions are prescribed in the boundary value problem being solved, then for a linearly elastic body,

$$\int_\tau U \, dA = \tfrac{1}{2} \int_\Sigma \mathbf{T}.\mathbf{U} \, ds. \qquad (45)$$

The traction $\mathbf{T}$ can be split into components T_N and T_T in the local coordinate axes T_N at any point of the perimeter, where N is the inwards facing normal. The stress components at the surface are $\sigma_{NN} = -T_N$ and $\sigma_{TN} = -T_T$. The displacement vector $\mathbf{U}$ can be similarly split into components U_N and U_T. Hence, from Equations 44 and 45 the potential energy, V, is

$$V = \tfrac{1}{2} \int_\Sigma (\sigma_{NN} U_N + \sigma_{TN} U_T) \, ds. \qquad (46)$$

When boundary elements with displacement discontinuities are used, Equation 46 must be interpreted with care, and the following two cases are distinguished.

(a) For a closed boundary: The convention is used that the positive side of the displacement discontinuity is on the inside of the boundary when the boundary is transversed in an anti-clockwise direction (Fig. 3a). Hence, to evaluate the potential energy of the body inside the boundary the displacements U_N^+ and U_T^+ must be evaluated on the boundary segments, and used in Equation 46. Conversely, for a cut-out hole in an infinite body, the boundary of the hole should be transversed in

a clockwise manner, so that U_N^+ and U_T^+ can still be used to evaluate the potential energy of the body.

(b) For a crack in an infinite body: Both sides of the displacement discontinuity of magnitude $b_T + i b_N$ supply energy to the body, so Equation 46 should be used with b_T and b_N replacing U_T and U_N, respectively.

When constant elements are used, it is assumed that both the stress components and the displacement components remain equal to their mid-segment values over the whole length of each boundary segment. Hence, the integral in Equation 46 can be replaced by a summation over all elements, with ds being replaced by the element length. When linear or crack-tip elements are used for crack problems, it is assumed that the stress components have their average values along the whole of each boundary segment, so that the potential energy can be calculated by multiplying this by the average value of the displacement jump along the boundary segment.

2.5.2. Meaning of the potential energy changes

For a purely elastic body containing a crack length, a, and for which the potential energy per unit thickness is V, the so-called "strain energy release rate", G, is defined by

$$G = - \partial V / \partial a. \qquad (47)$$

The name is only appropriate for bodies loaded under fixed-grip conditions, and G should, in general, be called the potential energy release rate. G is a useful fracture mechanics parameter, from which the stress intensity factor, K, can be calculated using

$$K^2 = EG/(1 - v^2) \qquad (48)$$

where E is Young's modulus, under plane strain conditions, for a single-ended crack, or for a crack that is growing symmetrically at both ends.

For elastic–plastic materials there will be a plastic zone at the crack tip, so the energetics of crack growth must be reconsidered. Rice [16] has defined an integral, J, for a notch that is parallel with the x-axis

$$J = \int_\Gamma \left(U \, dy - \mathbf{T} . \frac{\partial \mathbf{U}}{\partial x} \, ds \right), \qquad (49)$$

where Γ is now a curve that runs from the lower notch surface anti-clockwise around the crack tip

to the upper notch surface. Rice showed that

$$J = - \partial V / \partial a, \qquad (50)$$

where V is now the potential energy per unit thickness of the elastic region. Thus, the same quantity as in Equation 47 can still be used as a fracture mechanics parameter. This analysis by Rice [16] is strictly applicable only for non-linear elastic bodies, so it can only be applied to elastic–plastic bodies where the applied loads never decrease, so that there is never any reverse plastic yielding (which would prevent the strain being uniquely related to the stress).

Rice did not consider the situation of a crack remaining stationary while the yielded zone at the head of it grows, or of a yielded zone growing in the absence of a crack. If the size of the yielded zone is measured by a length R, then the quantity $- \partial V / \partial R$ may be a parameter that can be used to predict yielded zone growth. If equilibrium thermodynamics is applied to the elastic region in an elastic–plastic problem, then the principle that the equilibrium state of the region occurs when its free energy is minimized could be interpreted such that the yielded zone will grow only as long as $- \partial V / \partial R$ is positive.

3. Results
3.1. Comparison of elements for the growth of a central crack

When a central crack (extending from $x = -a$ to $x = a$ along the x-axis) in an infinite sheet is subjected to an internal pressure, p, the stored elastic energy of the sheet is given by

$$W = \pi a^2 p^2 (1 - v^2)/E \qquad (51)$$

and the crack-opening profile is given by the displacement

$$U_y = 4(1 - v^2) \frac{p}{E(a^2 - x^2)^{1/2}}, \qquad (52)$$

for $-a < x < a$ and $y = 0$. Any numerical solution to this boundary value problem should give energies and displacements that approximate to these results, the degree of approximation improving as the number of elements increases. This is shown to be the case in Table II.

It can be seen from Table II that the errors are also reduced with the use of better element types, and that calculations of G, which are made using the increment in V, when the number of elements is incremented by one, are more accurate than

Element type	Number of elements	W/a^2	$G_{\mathrm{I}}/\bar{a}$	$K_{\mathrm{I}}/\sqrt{a}$
Constant	4	12.5	5.6	
	9	5.6	2.9	
	25	2.0	1.0	
Linear	4	-3.6	-0.9	
	9	-1.2	-0.3	
	25	-0.2	-0.01	
Linear + crack-tip	4	0.5	-0.08	-2.7
	9	0.07	-0.05	-1.1
	25	-0.02	-0.02	-0.3

those of V. The signs of the discrepancies are explained by looking at the predicted crack profiles for 4-element cracks shown in Fig. 7. The constant element model largely ignores the local stress fields of the "dislocations" at the ends of the elements, particularly that at the end of the crack, so that, in the model, the rectangular end of the crack is too wide. The consequence of this is that the area inside the crack profile (representing the stored energy) is larger than the area under the analytic crack shape. On the other hand, the linear element model gives a good approximation to the crack shape except near the crack tip where it "cuts the corner", and hence underestimates the stored elastic energy.

The last column of Table II shows that estimating K from the opening of a single crack-tip element is not as accurate a method of estimating
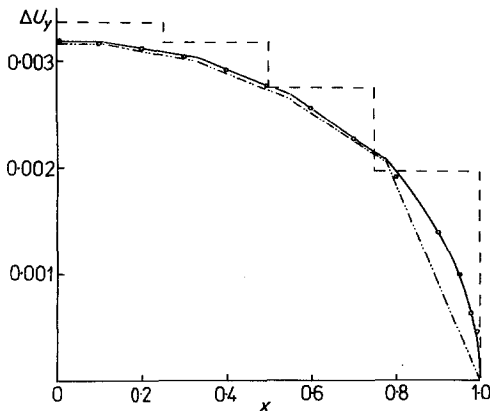
fracture mechanics parameters as the energy methods, but that it gives acceptable errors, $< 1\%$, when the total number of elements is greater than ten.

3.2. Growth of an infinite array of edge cracks

A more complex problem than that discussed above is the infinite array of edge cracks, modelled by the repeating constant elements shown in Fig. 5d. The analytical solution to this problem is known [17] even if the integrals involved must be evaluated numerically. The limiting case of the crack length, a, being much smaller than the crack separation, s, approximates to the single edge crack for which [18]

$$G_{\mathrm{I}} = 1.9858(1 - \nu^2)\sigma^2 2a/E, \qquad (53)$$

where σ is the tensile stress at infinity.

The other limiting case, where $a \gg s$, is equivalent to that of a long longitudinal crack growing in a pressurized pipeline for which the "strain energy release rate" is given by

$$G_{\mathrm{I}}^\infty = S(1 - \nu^2)\sigma^2/2E, \qquad (54)$$

where S is the circumference of the pipe in the pipeline case. Fig. 8 shows a comparison between Bowie's calculations [17], and the repeating constant element calculations. Both the strain energy release rate and the crack length are normalized by dividing by the crack separation. The agreement between the two calculations is good and they show that the strain energy release
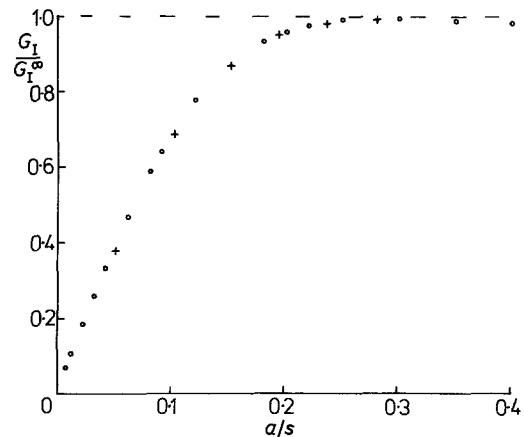

Figure 7 Modelling the crack opening of a centre crack in an infinite plate under tension. $----$ constant elements; $-\cdot\cdot-\cdot\cdot-$ linear elements; $\underline{\qquad}$ linear plus crack-tip elements. oooo analytical values, for the parameters of Table II, and $a = 1.0$ m.

Figure 8 Potential energy release rate, G_{I}, (normalized with respect to G_{I}^∞ of Equation 54) plotted against crack length, a, (normalized with respect to crack separations), for an infinite array of edge cracks; $\circ$ results of this paper, $+$ results of [17].

rate reaches a plateau value once the crack length exceeds 30% of the crack separation.

3.3. Growth of linear yielded zones from a central crack under plane stress conditions (Dugdale model)

The simplest type of elastic–plastic problem is one where the yielded zone is confined to a line (in two-dimensions), which simply extends as the applied load increases, and in which the stresses in the plastic zone are constant. The Dugdale model [19] is applicable to yielding in thin sheets of material in which plane stress conditions exist in the plastic zone. A central crack of half-length a will have at each end a yielded zone of length R, across which the tensile stress is σ_0 (the appropriate yield stress) and

$$R/a = \sec(\pi\sigma_\infty/2\sigma_0) - 1, \qquad (55)$$

when the stress component applied at infinity, perpendicular to the crack, is σ_∞. Dugdale solved this problem by finding the stress intensity factor K_A for a central crack of length $2(a + R)$ that has an internal pressure σ_∞, and the stress intensity factor K_B for the same crack with surface tractions of σ_0 applied for $a + R > |x| > a$. On adjusting the ratio R/a until $K_A + K_B = 0$, Equation 55 is obtained. It can be shown that this condition of no stress singularity at the yielded zone tip also does not violate Tresca's yield criterion in the surrounding elastic material.

It is not possible with the linear boundary element model to use Dugdale's approach in order to determine the equilibrium yielded zone length, R. Two alternative methods can be used:

(a) The yielded zone can be increased in length by adding further elements until it is predicted that the end element has a negative normal displacement discontinuity, b_N. As this corresponds to a physically inadmissable situation in the elastic–plastic solid being modelled, the yielded zone growth must have ceased at the previous increment.

(b) The rate of decrease of potential energy with yielded zone length $- \partial V/\partial A$ can be evaluated. When this is no longer positive it is postulated that the yielded zone will stop growing. In this state, the stored elastic energy, in the elastic region surrounding the yielded zone, has reached its maxumum value.

When constant elements were used then Alternative b was found to be the first to operate,

TABLE III Line yielded zones from a central crack

Stress σ_∞/σ_0	R/a			
	Equation 55	Linear elements	Constant elements	Element length
0.2	0.051	0.050	0.045	0.005
0.3	0.122	0.121	0.112	0.01
0.4	0.236	0.232	0.222	0.01
0.5	0.414	0.417	0.40	0.02

whereas when linear elements were used both criteria for the zone to stop growing came into effect simultaneously. The accuracy of the experimental results is compared with Equation 53 in Table III. If Alternative b is used it is possible to interpolate between results to get a more precise estimate of R.

Table III shows that the linear boundary elements give a sufficiently accurate result. As a further check, the predicted opening profile of the crack and yielded zone is compared in Fig. 9, for $\sigma_\infty/\sigma_0 = 0.3$, with the analytical expressions given in [20] for the Dugdale model. The agreement in profile is good.

Finally, both the stored elastic energy and the total dissipated energy have been calculated analytically by Weertman [21] for the Dugdale model. Using the set of parameters $\sigma_\infty = 5 \times 10^7 \, \text{N m}^{-2}$, $\sigma_0 = 1.0 \times 10^8 \, \text{N m}^{-2}$, $\nu = 0.45$, $E = 3 \times 10^9$ and $a = 1 \, \text{m}$ the difference between the energies calculated analytically and those calculated from the equilibrium length of the linear element model was found to be 0.1%, as shown in Table IV.
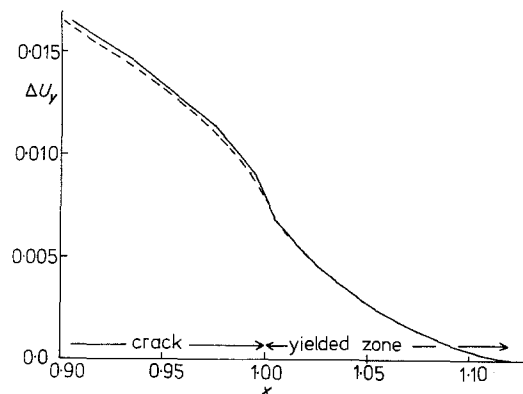

Figure 9 Crack and yielded zone opening displacement for a line yielded zone where $\sigma_\infty/\sigma_0 = 0.3$, $\sigma_\infty = 30 \, \text{MN m}^{-2}$, $E = 3 \, \text{GN m}^{-2}$, $\nu = 0.45$. – – – – analytical results; ——— results using linear elements.

TABLE IV Energies of a central crack in an infinite sheet plus equilibrium Dugdale yielded zone

Parameter	Analytical value	Value from linear element calculation
Potential energy (MJ)	2.346†	2.345*
Plastically dissipated energy (MJ)	0.6241	0.6236

*For a yielded zone of length $R/a = 0.42$, made up from 21 elements.
†Using $V = -8(1 - \nu^2)\sigma_0^2 a^2 \log \sec (\pi\sigma_\infty/2\sigma_0)/E\pi$.

3.4. Growth of a plane strain plastic zone from a circular hole in an infinite sheet under tension

This is an example of a more complex elastic–plastic problem, of the type usually tackled using finite element methods. In general, the shape of the plastic zone is unknown in problems of this kind, but, for certain materials that exhibit little work hardening, the yielded zone has been observed experimentally to have a particularly simple shape [9]: one that corresponds to a simple slip-line field of orthogonal logarithmic spirals (Fig. 2b). The yielded zone was observed to grow by increasing the angle, α, of the outermost slip lines, so, in modelling the yielding process from the circular hole in a sheet, α was taken as the disposable parameter. Using constant displacement elements around the outer boundary of the hole and the yielded zone, the elastic boundary value problem was solved for a range of α-values. Fig. 10 shows how the potential energy of the elastic region varies with α for a particular ratio of the tensile
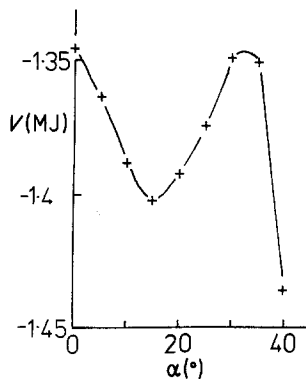
stress at infinity to the shear yield stress of the material. Using Alternative b of Section 3.3., the equilibrium yielded zone size is predicted to occur when the potential energy is a maximum at an angle, α, of 15°. To discover if this is a realistic result, the stresses in the elastic region outside the yielded zone were calculated for a range of α-values. It was found that the Tresca (or Von Mises) yield criterion was violated in the "elastic" region unless the yielded zone had an angle of extent, α, of about 20°. Hence, the two methods of predicting the equilibrium yielded zone size do not exactly coincide in this case.

3.5. Predictions of crack growth directions

For the simple situation of a central crack at an angle, β, to the uniaxial tension applied at the ends of an infinite sheet (see the inset in Fig. 11) the use of linear plus crack-tip boundary elements gives good predictions of crack growth direction. Even when only 10 equal-length elements are used to model half the crack, the ratio of the stress intensity factors K_{II}/K_I, found from the displacement discontinuity of the crack-tip element, is exactly equal to the analytical value of $\cot \beta$. The subsequent solution of Equation 43 will then give the crack growth direction according to the
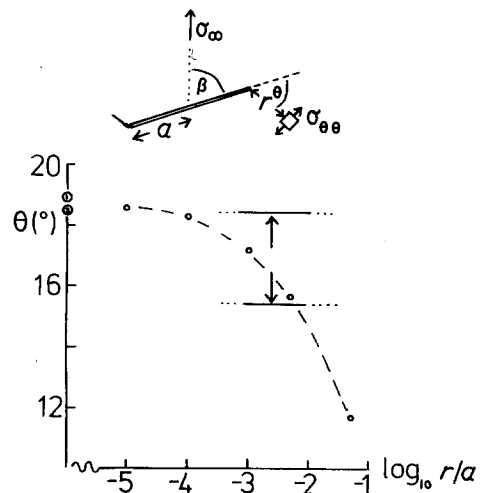

Figure 10 Variation of potential energy, V, with yielded zone extent, α, for a notch of radius 1 m (Fig. 2b) predicted using constant displacement elements. $\sigma_\infty = 40\,\mathrm{MN\,m^{-2}}$; shear yield stress $30\,\mathrm{MN\,m^{-2}}$, $E = 3\,\mathrm{GN\,m^{-2}}$; $\nu = 0.45$.

Figure 11 Growth directions of a crack initially at an angle $\beta = 80°$ to the applied stress. The band shows the experimental results [14], and the curve is the predicted angular position of maximum $\sigma_{\theta\theta}$ as a function of the radial distance, r, from the crack tip. Position 1 is the prediction of the $\sigma_{\theta\theta}$ criterion at $r = 0$, and Position 2 is the strain energy criterion for $\nu = 1/3$.
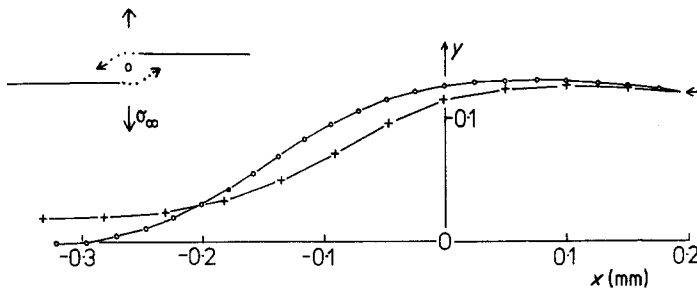
Figure 12 Growth path predictions for two off-set, initially-parallel cracks 2.3 mm long (see inset) +++ constant displacement elements searching for $\sigma_{\theta\theta}$ at radius, $r = 0.05$ mm, ooo linear elements. 0 is the centre of symmetry of the two cracks.

maximum $\sigma_{\theta\theta}$ stress hypothesis. However, when the same problem was tackled using 10 equal-length constant-displacement elements to model the half-crack, and searching for the maximum $\sigma_{\theta\theta}$ at a radius equal to the element length, large errors occurred. For example, at a crack orientation of $\beta = 60°$ the predicted growth direction was $\theta = 32°$, whereas the analytical value as $r \to 0$ is $43°$. This is a severe test, as the crack deviates sharply from its previous direction.

Sih [14] has discussed the agreement between experimental measurements of the crack growth direction, using the glassy thermoplastic poly-methylmethacrylate (PMMA), and the predictions of the maximum stress and the strain energy density criteria. As a by-product of the stress analysis carried out here, it was possible to find the position of the maximum stress, $\sigma_{\theta\theta}$, at various radial distances, r, from the crack tip. Fig. 11 shows that, for the crack orientation $\beta = 80°$, the position of the maximum changes considerably in the neighbourhood of the crack tip (for example, for $r/a < 0.01$). The range of experimental values observed is also indicated; it is likely that these were measured at a radial distance of between 10^{-3} and 10^{-2} a. It is also known [22] that before a crack in PMMA can grow, a craze of length $\sim 30 \mu$m forms at its tip, and that the initial path of crack growth follows the craze plane. For these reasons it seems highly unlikely that the experiments with PMMA are accurate enough to favour the maximum stress criterion over the strain energy criterion or vice versa. It can be concluded that either criterion gives a good first approximation to the crack growth direction.

We have recently analysed a more complex crack-growth situation using constant displacement elements [23]: that of two parallel but off-set cracks in an uniaxial stress field (Fig. 12). Repeating the calculation using linear elements and crack-tip elements at both ends is a useful check of the original calculation and it provides a better

insight into the changes in the fracture mechanics parameters. The predicted crack-growth path in Fig. 12 is almost identical to that of the earlier constant element model. This shows that the presence of a single dislocation at the end of the "crack" in the constant element model does not badly affect the predicted crack growth path so long as the position of $\sigma_{\theta\theta}$ is searched for at a radius equal to the element length and provided that the crack path only changes direction gradually. Using the crack-tip elements enables the separate stress intensity factors, K_{I}, at the inner and outer crack tips to be plotted against crack growth, see Fig. 13 (both inner crack tips are assumed to grow, whereas the outer crack tips do not, and the model maintains a two-fold rotational symmetry axis at the origin). The K_{II} values of both crack tips are less than 10% of the K_{I} values. Fig. 13 shows that K_{I} of the inner crack tips reaches a maximum value just after the crack projections overlap on the x-axis, then the value decreases rapidly. However, the K_{I} value of the outer crack tips increases slowly and steadily as the crack pair approximates more and more to a large single crack. A further
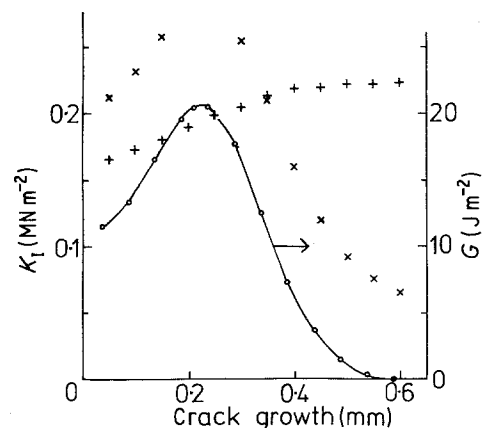

Figure 13 Variation of fracture mechanics parameters for the crack growth shown in Fig. 12. $+ K_{\mathrm{I}}$ of outer crack tips, $\times K_{\mathrm{I}}$ of inner crack tips, $\circ$ G for whole system. $\sigma_\infty = 3\,\mathrm{MN\,m}^{-2}$, $E = 3\,\mathrm{GN\,m}^{-2}$, $\nu = 0.45$.

interesting feature is that the "strain energy release rate", G, varies in a way that is not directly related to either of the K_I values, and in fact becomes zero after 24 growth steps, when both K_I values are non-zero. It can be said that the still-open innermost crack tips are "stealing" energy from the centres of the other cracks, and that the net result of this process is a zero change in the potential energy of the system. It shows clearly that when there are two crack tips in dissimilar stress field surroundings, then the global fracture mechanics parameter G is no longer uniquely linked to the local crack tip stress field parameter K by Equation 48, as is the case for a single central crack.

4. Discussion

It has been shown that boundary elements using linear variations in displacement discontinuity give better approximations to the analytical solutions of crack problems than do constant displacement elements. The disadvantage of this former method is that the computation time needed for the predictions is increased by two to three times. However, less elements are needed in order to achieve the same degree of accuracy. Crack-tip elements are useful in that, as well as improving the accuracy of the stress field simulation at the crack tip, they allow a direction evaluation of the fracture mechanics parameters K_I and K_{II} without necessitating the evaluation of the potential energy changes.

Compared with the finite element method the data input to the boundary element method is much simpler for crack problems in infinite sheets; the solution time is relatively fast provided that the number of elements is kept small. For example, using an ICL 1906 A computer, a problem using 33 linear boundary elements (each of which had 3 images because of the symmetry of the body) was solved in 84 sec; an evaluation of the stress field at 100 points took 46 sec.

The problem of the equilibrium length, R, of a line yielded zone was solved using the criterion $-\partial V/\partial R = 0$, and this was shown to give the same results as Dugdale's solution. This criterion can be contrasted with Rice's J integral, which has a value of $-\partial V/\partial a$ for the growth of a crack with an equilibrium-sized yielded zone. Thus, the potential energy calculations, that emerge readily from the boundary element method, are useful in both plasticity and fracture mechanics calculations. When a more

complex elastic–plastic problem having a yielded region was analysed the criterion $-\partial V/\partial R = 0$ no longer gave an exact prediction of the yielded zone size that would avoid violating the yield criterion. However, the boundary element method is still a rapid way of analysing the stresses that correspond to the observed pattern of yielding in a particular material. It is certainly a better method than slip line field analysis when the observed plastic zone is seen to be surrounded by elastic material, since slip line field analysis assumes a rigid–plastic material and the slip lines cannot end in the interior of the body.

It was possible to make accurate predictions of crack growth directions using crack-tip elements and it would appear that the maximum circumferential stress criterion is appropriate to glassy materials like polymethylmethacrylate (PMMA). Further tests of the usefulness of the boundary element method are described in the accompanying paper on its application to crazing in glassy plastics [24].

References

1. B. A. BILBY and J. D. ESHELBY, in "Fracture", Vol. 1, edited by H. Liebowitz (Academic Press, New York and London, 1968).
2. R. W. LARDNER, "Mathematical Theory of Dislocations and Fracture" (University of Toronto Press, Toronto, 1974).
3. S. L. CROUCH, *Int. J. Numer. Meth. Eng.* **10** (1976) 301.
4. M. J. MARCINKOWSKI and E. S. P. DAS, *Int. J. Fracture* **10** (1974) 81.
5. M. P. CLEARY, *Int. J. Numer. Meth. Eng.* **10** (1976) 679.
6. D. S. DUGDALE and A. RUIZ, "Elasticity for Engineers" (McGraw Hill, New York, 1971).
7. C. A. BREBBIA, "The Boundary Element Method for Engineers" (Pentech Press, Plymouth, 1978).
8. M. ISIDA, in Proceedings of the Conference on Numerical Methods in Fracture Mechanics, edited by A. R. Luxmoore and D. R. J. Owen, (University College, Swansea, 1978).
9. N. J. MILLS, *J. Mater. Sci.* **11** (1976) 363.
10. N. I. MUSKHELISHVILI, "Some Basic Problems of the Mathematical Theory of Elasticity" (Noordhoff Publishing Co., Leyden, The Netherlands, 1953).
11. V. VITEK, *J. Mech. Phys. Sol.* **24** (1975) 67.
12. A. H. ENGLAND, "Complex Variable Methods in Elasticity" (John Wiley and Sons, New York, 1971).

13. W. T. READ and W. SHOCKLEY, *Phys. Rev.* **78** (1950) 275.
14. G. C. SIH (Ed.), in "Three-dimensional Crack Problems", Vol. 2 (Noordhoff Publishing Co., Leyden, The Netherlands, 1975).
15. R. P. KAMBOUR, *J. Polymer Sci. Macromol. Rev.* **7** (1973) 1.
16. J. R. RICE, *J. Appl. Mech. Trans. ASME* **E35** (1968) 379.
17. O. L. BOWIE, in "Methods of Analysis and Solution of Crack Problems", edited by G. C. Sih (Noordhoff Publishing Co., Leyden, The Netherlands).
18. W. T. KOITER, *Proc. K. Ned. Akad. Wet.* **B59** (1956) 365.
19. D. S. DUGDALE, *J. Mech Phys. Sol.* **8** (1960) 100.
20. J. N. GOODIER and F. A. FIELD, in "Fracture of Solids", edited by D. C. Drucker and J. J. Gilman (John Wiley and Sons, New York, 1963).
21. J. WEERTMAN, Proceedings of the International Conference on Fracture, Sendai, Japan, 1966 Vol. 1 (Japan Society, Tokyo, 1966) p. 153.
22. H. R. BROWN and I. M. WARD, *Polymer* **14** (1973) 469.
23. N. J. MILLS and N. WALKER, *Eng. Fracture Mech.* **13** (1980) 479.
24. N. J. MILLS, *J. Mater. Sci.* **16** (1981) 1332.